Materials Chemistry and Physics 269 (2021) 124743

Contents lists available at ScienceDirect

Materials Chemistry and Physics

journal homepage: www.elsevier.com/locate/matchemphys

Copper sulfide nanoparticles produced by the reaction of N-alkyldithiocarbamatecopper(II) complexes with sodium borohydride

Eder I. Duran-García [a,b], José Martínez-Santana [a,b], Nayely Torres-Gómez [c], Alfredo R. Vilchis-Nestor [d], Iván García-Orozco [b,*]

[a] Universidad Autónoma del Estado de México, Facultad de Química, Programa de Maestría en Ciencia de los Materiales, Paseo Colón esq. Paseo Tollocan s/n, 50120, Toluca, CP 50120, Mexico

[b] Universidad Autónoma del Estado de México, Facultad de Química, Laboratorio de Investigación y Desarrollo de Materiales Avanzados (LIDMA), Carretera Toluca-Atlacomulco Km 14.5, Unidad San Cayetano, Toluca, México, CP 50200, Mexico

[c] Tecnológico Nacional de México, Campus Toluca. Av, Tecnológico s/n, Colonia Agrícola Bellavista, Metepec, Edo. De México, C.P. 52149, Mexico

[d] Centro Conjunto de Investigación en Química Sustentable UAEM-UNAM, Facultad de Química, UAEM, Carretera Toluca-Atlacomulco Km 14.5, Unidad San Cayetano, Toluca, México, CP 50200, Mexico

HIGHLIGHTS

- A chemical strategy to obtain Cu_xS nanoparticles.
- Dithiocarbamate ligand remains in the nanoparticle.
- Cu_9S_5 and CuS (or Cu_2S) phases present in the particles.
- Discrete size distribution of Cu_xS-NP.
- Cu_xS-NP band gaps reflect quantum size effect.

GRAPHICAL ABSTRACT

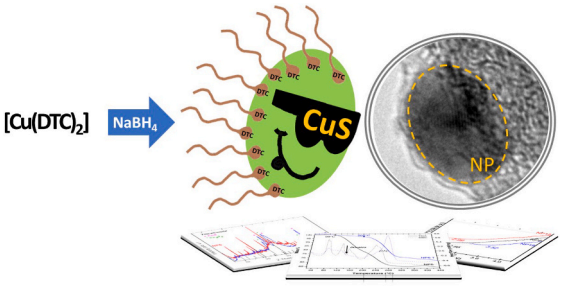

ARTICLE INFO

Keywords:
Copper sulfide
Nanomaterials
N-alkyldithiocarbamate
Surface ligand
Semiconductor materials

ABSTRACT

Copper sulfide nanoparticles (Cu_xS-NP) surface-stabilized by dithiocarbamate (DTC) molecules were obtained with controlled size and shape by a novel one-step wet chemical methodology for the chemical transformation of a single-source precursor. The reaction of N-alkyldithiocarbamatecopper(II) complexes with $NaBH_4$ in ethanol solution produces Cu_xS-NP of hexyl- (NP6), dodecyl- (NP12), and octadecyl- (NP18) carbon chains. The characterization of the particles was carried out by IR spectroscopy, Diffuse Reflectance Spectroscopy, Powder X-ray Diffraction, Thermal Analyses, and Transmission Electron Microscopy. The Cu_xS-NP are capped with DTC ligands which can tune the particle size. The Cu_xS phases obtained are closely related to the DTC chains length since NP6 produces Cu_9S_5 and CuS, NP12 yields Cu_9S_5 and Cu_2S, finally, Cu_9S_5 and CuS are produced with NP18. In all the cases, the particles have a quasi-spherical shape, and the length of the DTC chain controls the particle size. The band gap of the Cu_xS-NP is around 3.0 eV, calculated by the Tauc baseline method, confirming their semiconductor nature and strong quantum confinement.

* Corresponding authors. Universidad Autónoma del Estado de México, Facultad de Química, Laboratorio de Investigación y Desarrollo de Materiales Avanzados (LIDMA), Carretera Toluca-Atlacomulco Km 14.5, Unidad San Cayetano, Toluca, México, CP 50120, Mexico.
E-mail address: igarciao@uaemex.mx (I. García-Orozco).

https://doi.org/10.1016/j.matchemphys.2021.124743
Received 12 January 2021; Received in revised form 14 April 2021; Accepted 18 May 2021
Available online 21 May 2021

1. Introduction

The copper sulfide nanoparticles (Cu_xS-NP) is a p-type semiconductor material that has been used as a photocatalyst in ultraviolet–visible (UV–vis) and infrared (IR) regions [1], as a photothermal switch against atherosclerosis [2], as antibacterial agent [3], as electrocatalyst for water oxidation [4], in biomedical applications [5], among other promising applications [6]. For achieving the desired application, it is important to control the structure and phases of the material by its preparation methods. The synthesis techniques of Cu_xS-NP could be classified in two general ways, regarding the sources of the copper and sulfur atoms: those with two precursors (one for copper and one for sulfur atoms) [7–10], and those with a single-source precursor (SSP), including both required atoms [6]. The use of a single-source precursor is a robust approach for nanoparticle synthesis. This approach has potential advantages: the desired atoms are in only one molecule, air, and moisture stable, avoiding the incorporation of impurities on the material. N, N-dialkyl dithiocarbamatecopper(II) complexes are often the most frequent SSP to obtain copper sulfide nanoparticles [11–18]. Thermal decomposition of the SSP produces an effective control of the phases, size, and structure of the Cu_xS-NP. However, in all cases is necessary the addition of a passivating agent to avoid coalescence of the obtained particle, because the dithiocarbamate completely degrades with thermal treatment.

The use of N-alkyldithiocarbamate copper complexes in the copper sulfide preparation is unexplored despite their similar stability and advantages than N, N-dialkyl complexes. N-alkyldithiocarbamate metal complexes have been commonly used to obtain metal sulfides by thermolysis. For this procedure, cadmium sulfides [19 20 21], nickel sulfide [22,23], iron sulfides [24], and zinc sulfide [25 .26] were obtained, even though there are no reports for copper sulfide. The present work aims to obtain ligand-modified metal sulfides nanoparticles, allowing better size control and improved affinity to non-polar surfaces. In this study, we aimed to prepare Cu_xS-NP using soft conditions avoiding toxic solvents, high temperatures, surfactants, structure-directing agents, stabilizers, etc. It is well known that surfactants are used to control the size and morphology of nanomaterials, as in Pt nanoparticles [27], nanosilica powders [28], iron oxide nanoparticles [29], iron nanoclusters [30], among other examples. For Cu_xS-NP, the large carbon number of alkyl chains increases the size of Cu_xS nanocrystals by thermal decomposition of dialkyldithiophosphates copper(II) complexes [31]. The use of a single-source precursor as an N-alkyldithiocarbamate copper complex in a chemical strategy prompted us to develop the technique. For this reason, N-alkyl dithiocarbamatecopper(II) complexes with long carbon chains were used in this work as a single-source precursor of copper sulfide nanoparticles by the chemical reaction of sodium borohydride with N-alkyldithiocarbamatecopper(II) complexes. Controlled size and shape Cu_xS-NP were obtained, with the main advantage that DTC ligands remain in the obtained particle. Three different lengths of carbon chains were evaluated, to assess their impact on the size and phase of the Cu_xS particles. The semiconductor behavior was evidenced by its band gap values (E_g), nearing the visible region, with strong quantum confinement due to the small size of the particles.

2. Experimental section

2.1. Material and methods

All reagents were analytical grade and used without further purification. Bis(N-hexyldithiocarbamate)copper(II) (CuD6), Bis(N-dodecyldithiocarbamate)copper(II) (CuD12), and Bis(N-octadecyldithiocarbamate)copper(II) (CuD18) were prepared by our reported methodology [32]. The annealing treatment was performed in a Quincy Lab 20 GC gravity convection lab oven preheated at 180 °C. The infrared spectra (IR) were recorded on a Bruker Tensor 27 FTIR spectrometer with an ATR accessory in the range of 4000 to 400 cm^{-1}. The powder X-ray diffraction data were obtained in a Bruker D8 Advance diffractometer using Ni-filtered Cu-K_α radiation ($\lambda = 1.541$ Å); tube conditions: 30 kV and 30 mA, 2θ: 5–80°, step size: 0.03°, step time: 32 s. The diffractograms were analyzed using the program PANalytical X'Pert HighScore Plus (version 2.2b), which let compare with the ICDD powder X-ray diffraction pattern database (PDF Release 2). Thermograms were obtained with a Netzsch model STA 449 F3 Jupiter thermal analyzer from 20 to 550 °C, with a heating rate of 10 °C/min, in a nitrogen atmosphere (purity of 99.999%). The nanoparticle morphology and size were studied with a JEM-2100 transmission electron microscope from JEOL using an accelerating voltage of 200 kV and LaB_6 filament (point resolution of 2.3 Å). Moreover, the crystalline structure of the Cu_xS nanoparticles was determined with a field emission transmission electron microscope JEM-2010F from JEOL operated at 200 kV of accelerating voltage (resolution of 1.9 Å). One drop of each type of Cu_xS nanoparticles, dispersed in 2-propanol was placed in a Cu grid coated with carbon, and allowed to dry at room conditions to perform. To obtain statistically consistent information on the particle size distribution was employed ImageJTM software analyzed around 200 to 210 particles per histogram.

2.2. Synthesis of Cu_xS nanoparticles

The synthesis of copper nanoparticles of N-hexyldithiocarbamate (NP6) follows a general methodology: an ethanol solution of carbon disulfide (0.9 mL, 9.3 mmol) was added to a mixture of n-hexylamine (0.6 mL, 4.5 mmol) and NaOH (4.5 mmol) in ethanol. An ethanol solution of $Cu(NO_3)_2{\cdot}2.5H_2O$ (0.384 g, 2.25 mmol) was added to the reaction, stirring for 60 min. The obtained yellowish powder was filtered and dried overnight under a vacuum. The complex was suspended in 10.0 mL of ethanol, and a $NaBH_4$ ethanolic solution (160 mg, 4.2 mmol) was added under constant stirring. The brownish precipitate was filtrated in a vacuum, washed with deionized water and ethanol, and dried at room temperature overnight. The same procedure was used for Cu_xS-NP with dodecyl chain (NP12), and octadecyl chain (NP18), using N-dodecylamine and N-octadecylamine, respectively. The annealing of the samples was carried out in a lab drying oven preheated at 180 °C. The samples were dried for 10 min (only 5 min for NP6, to prevent decomposition of CuS into copper sulfate) and subsequently allowed it to cool at room temperature in a desiccator. The annealed samples (NPT) were identified by NP6T, NP12T, and NP18T.

3. Results and discussion

3.1. Preparation of Cu_xS-NP

The dithiocarbamate stabilized Cu_xS-NP were obtained through the transformation of copper complexes CuDTC as a single molecular precursor, with a sodium borohydride ($NaBH_4$) ethanolic solution (Scheme 1). The use of recently prepared CuDTC avoids interferences from the copper salt precursor or the free dithiocarbamate ligand, obtaining the particles in high quantity. The sodium borohydride was used to reduce copper(II) to copper(I), with the aim to control the Cu_xS phase. Borohydride anion reacted with the water present in the reaction media to generate molecular hydrogen and borates. The molecular hydrogen reduced the ion copper(II) to copper(I), yielding the digenite phases as the majority Cu_xS phase [33]. Borohydride was decomposed into basic hydride ions[34 35], which reacted with the acid hydrogen atom H–N of the monoalkyl dithiocarbamate to form CuS by non-oxidative C–S bond cleavage [19]. An alkyl isothiocyanate (R–NCS in Scheme 1) was obtained as a byproduct of the reaction, which was identified by the IR spectrum (ν (SCN): 2100 cm^{-1}) in the residual solution. The copper(II) ion acts as a desulfurization agent of DTC to obtain the alkylisothiocyanates [36]. The rest of the molecule produces the Cu_xS with DTC still bonded by the copper atom. Therefore, the amount of borohydride is important for obtaining copper sulfide. Three different $NaBH_4$:CuDTC

ratios (2:1, 4:1, and 10:1) were evaluated, for each carbon chain (NP6, NP12, and NP18). The produced amount of NP6 keeps almost the same, despite the different relations used. Instead, for NP12 and NP18, the ratio 2:1 produced less amount of Cu_xS nanoparticles (approx. the half) than with ratio 4:1. It is important to note that the reaction with ratio 2:1 was not accomplished, because the obtained solid resemble the color of the precursor complex. A greater amount of borohydride was necessary to complete the reaction. The ratio 10:1 was not for practical applications because it generates a similar amount than ratio 4:1. The color of NP6 and NP12 was black-browned, but NP18 proved to be a greenish-black, possibly related to the nanometric size, as mentioned by Wills [37] and Zhou [38].

3.2. IR characterization of Cu_xS-NP

The dithiocarbamate ligand (DTC) remain bonding to the CuS after the synthetic reaction. In the infrared spectra (IR) of NP samples (Fig. 1), the signals at 2920, 2850, 1470, 940, and 670 cm^{-1} show the presence of the dithiocarbamate ligands on the surface of Cu_xS-NP. Only the NP6 spectrum shows a sharp band at 3270 cm^{-1} for the N–H stretching vibration [39 40], possible due to the number of C–H groups in respect to NP12 and NP18. The signal around 1460 cm^{-1} is characteristic of the thioureide stretching frequency C–N for the dithiocarbamate group [41]. The peaks from the nearby 930 cm^{-1} show the bonding mode of the dithiocarbamate to a metal ion [32 42]. The sharp band ca. 940 cm^{-1} demonstrates the symmetrical bidentate coordination of the dithiocarbamate group onto the Cu_xS-NP surface [43 44]. These two bands (C–N and C–S) change from the CuDTC complex to the Cu_xS-NP as can be seen in Table 1. The C–N and C–S bands respectively shift toward minor and higher wavenumbers, from the coordination compound to the CuS. The bonding order C–N decreases while the C–S increases when the nanoparticles are formed. The DTC ligand acts more like a mono-anion (b) than a di-anion (a) ligand (Scheme 2). Therefore, the DTC ligand carries out a lower donation of electron density to the metal center maybe copper has more electrons due to the reduction of Cu(II) to Cu(I), as well as the formation of copper sulfide, with a higher electron density than the copper(II) ion.

However, the samples do not only have DTC over the surface of Cu_xS-NPs. There are signals at 3240, 1340, 1270, 1250, 1130, 995, 820 cm^{-1} (Fig. 1) that correspond to Tincalconite [$Na_2B_4O_5(OH)_4{\cdot}3H_2O$], a product generated by the reaction of $NaBH_4$. The Tincalconite is hard to remove from the products and continues despite the various washings with distilled water and ethanol. For NP12 and NP18 sample spectra, a broad signal centered in 3300 cm^{-1} is related to surface adsorbed water, confirmed by the weak signal at 1640 cm^{-1}. Both are consistent with the crystallization water of the tincalconite structure.

3.3. Powder X-ray diffraction analyses of Cu_xS-NP

The powder X-ray diffraction analyses (XRD) of Cu_xS-NP show a crystalline nature of the samples (Fig. 2 – 4), mainly due to the presence of the tincalconite phase (JPCD card 71–1536) in the first instance. The

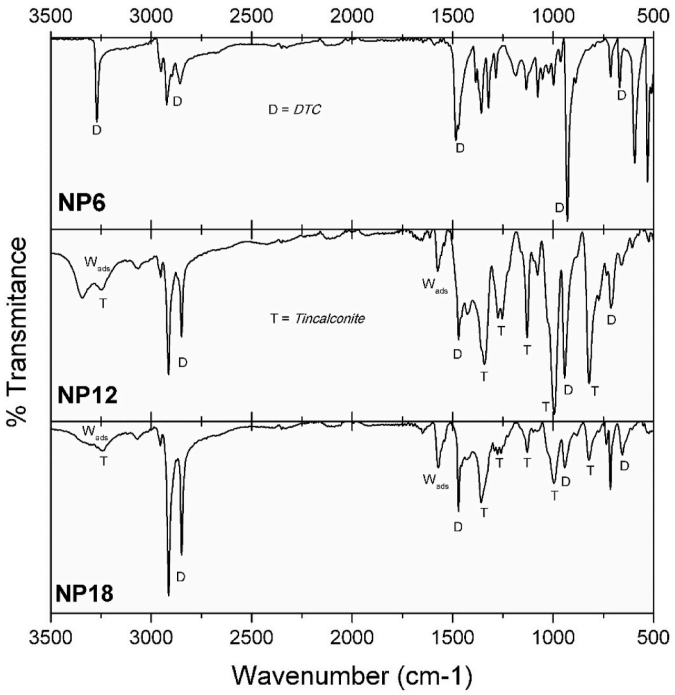

Fig. 1. *IR spectra of Cu_xS-NP recent synthesized NP6, NP12, and NP18.*

existence of an amorphous phase in the diffractograms is notable, which decreases in quantity as the chain grows: NP6 > NP12 > NP18. The longer the DTC chain, the more crystallinity is generated in the sample, probably due to weak interactions on the carbon chains. Some minor intensity broad peaks around 30° and 50° are consistent with the Cu_xS phases. It is important to note that the samples were washed several times with water and ethanol, which it is inefficient to eliminate all the residual compounds. The copper sulfide could be associated with Cu_xS particles with nanometric size, since the diffractogram present amorphous baseline and the broader peaks. It was not possible to calculate the particle sizes using the Scherrer formula due to the overlapping of the peaks in the diffractograms. The next treatment of the samples allowing identification of the Cu_xS phases (see Fig. 3).

3.4. Transmission electron microscopy of Cu_xS-NP

The morphological and structural characterizations of Cu_xS-NP were performed with Transmission Electron Microscopy (TEM) (see Fig. 4). From the TEM micrographs in Fig. 5, it can be observed that the precipitates are formed by nanoparticles with quasi-spherical shape.

TEM micrographs for NP6, NP12, and NP18 samples (Fig. 5A, E and 5I, respectively) display a uniform size of nanoparticles, with a quasi-sphere shape as the predominant morphology. However, the NP12 micrograph shows some ellipsoidal particles (Fig. 5E), and the NP18

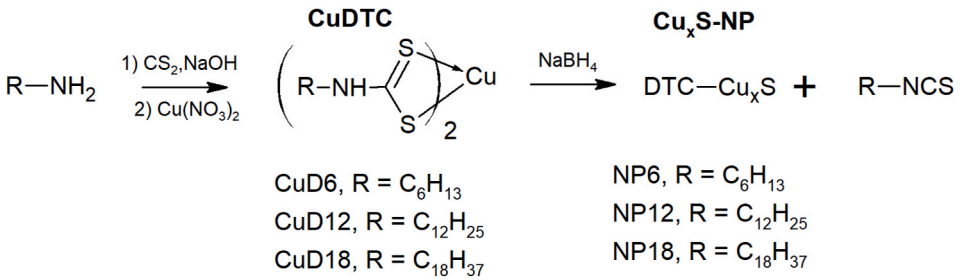

Scheme 1. General synthesis of Cu_xS-NP from the dithiocarbamate copper complexes CuDTC with different carbon chain: hexyl- (NP6), dodecyl (NP12), and octadecyl- (NP18).

Table 1
Principal IR signals (cm^{-1}) for the CuDTC complex (CuD6, CuD12, and CuD18) and Cu_xS-NP samples as synthesized (NP6, NP12 and NP18), and before annealing (NP6T, NP12T, and NP18T).

Vibration	CuD6	NP6	NP6T	CuD12	NP12	NP12T	CuD18	NP18	NP18T
(C–N) $_\nu$	1500	1484	1499	1489	1470	1424	1500	1471	1415 sh
(CS_2–Cu) $_\nu$	929	930	–	929	943	–	937	941	–
(-$(CH_2)_n$-) $_\rho$ ($n \geq 4$)	671	670	–	674	674	–	675	670	–

Note: ν - stretching, ρ - rocking, sh - shoulder.

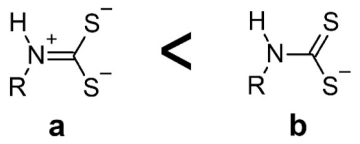

Scheme 2. Proposed forms of donation of DTC ligands.

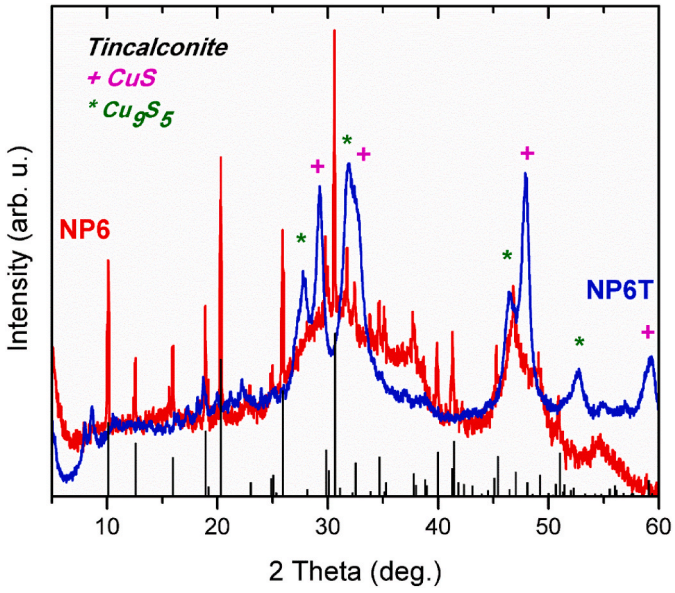

Fig. 2. X-ray diffractograms of Cu_xS-NP as synthesized (red NP6) and after annealing (blue NP6T). Tincalconite card (JPCD 71–1536) are showed by thin bars (black), and Cu_xS phases are depicted as marks (CuS JPCD 03–0724, Cu_9S_5 JPCD 040861). (For interpretation of the references to color in this figure legend, the reader is referred to the Web version of this article.)

micrograph (Fig. 5I) shows some agglomerates that could be produced by subtle interactions of the DTC carbon chain covering the nanoparticle, since the DTC passivate the surface of the nanoparticles, preventing the coalescence. From Fig. 5, it is observed that the morphological control is maintained, towards spherical or quasi-spherical particles, despite the size increment of the DTC carbon chain. A longer carbon chain causes a greater average size and better size distribution. To the other side, short carbon chains form a more stable layer onto the particle, limiting growth in particular planes, with less symmetrical structures. The DTC with longer carbon chains produce nanoparticles of greater average size than shorter carbon chains (Table 2, Fig. 5D, H, and 5L). Long-chain dithiocarbamates act as surfactants. In a polar solution (ethanol), they form micelles with the polar head pointing out. N-alkydithiocarbamatecopper(II) micelles form the nanoparticles by the reaction with sodium borohydride, influenced by the micelle size and hence, by the length of the carbon chain. The length of the DTC carbon chains controls the association of the fragment DTC-CuS, forming copper sulfide particles of nanometric size covered by a monolayer of DTC ligands [45], avoiding the bulk aggregation [40].

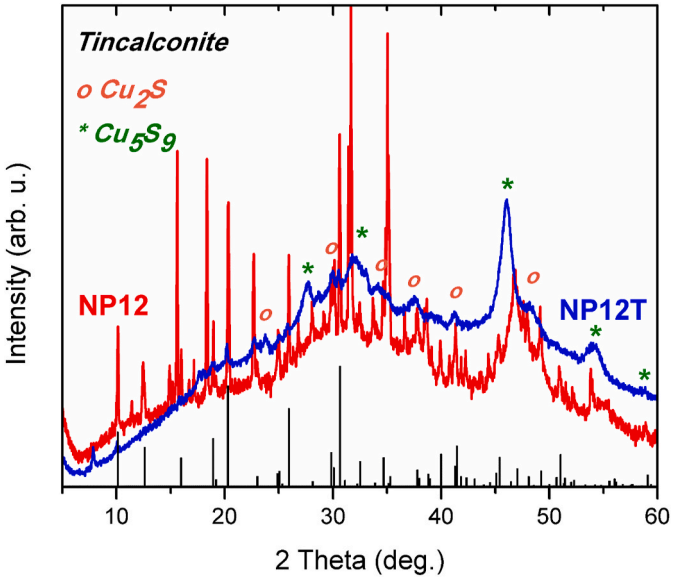

Fig. 3. X-ray diffractograms of Cu_xS-NP as synthesized (red NP12) and after annealing (blue NP12T). Tincalconite card (JPCD 71–1536) are showed by thin bars (black), and Cu_xS phases are depicted as marks (Cu_2S JPCD 02–1272, Cu_9S_5 JPCD 040861). (For interpretation of the references to color in this figure legend, the reader is referred to the Web version of this article.)

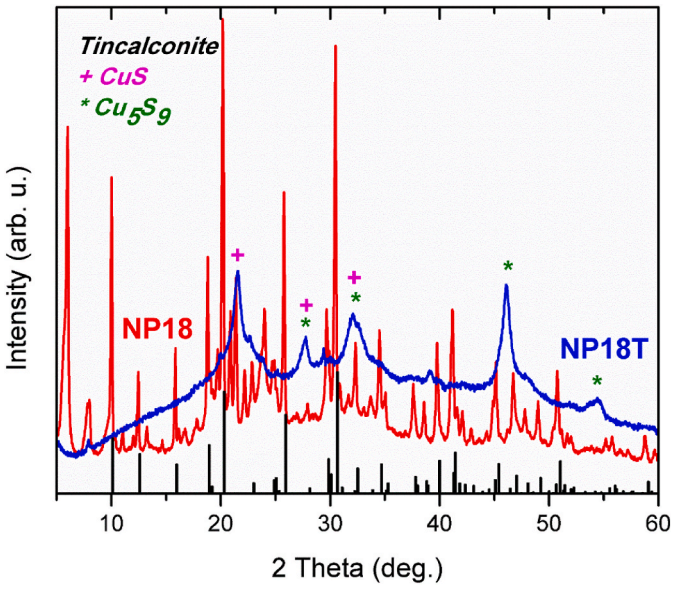

Fig. 4. X-ray diffractograms of Cu_xS-NP as synthesized (red NP18) and after annealing (blue NP18T). Tincalconite card (JPCD 71–1536) are showed by thin bars (black), and Cu_xS phases are depicted as marks (CuS JPCD 65–3929, Cu_9S_5 JPCD 040861). (For interpretation of the references to color in this figure legend, the reader is referred to the Web version of this article.)

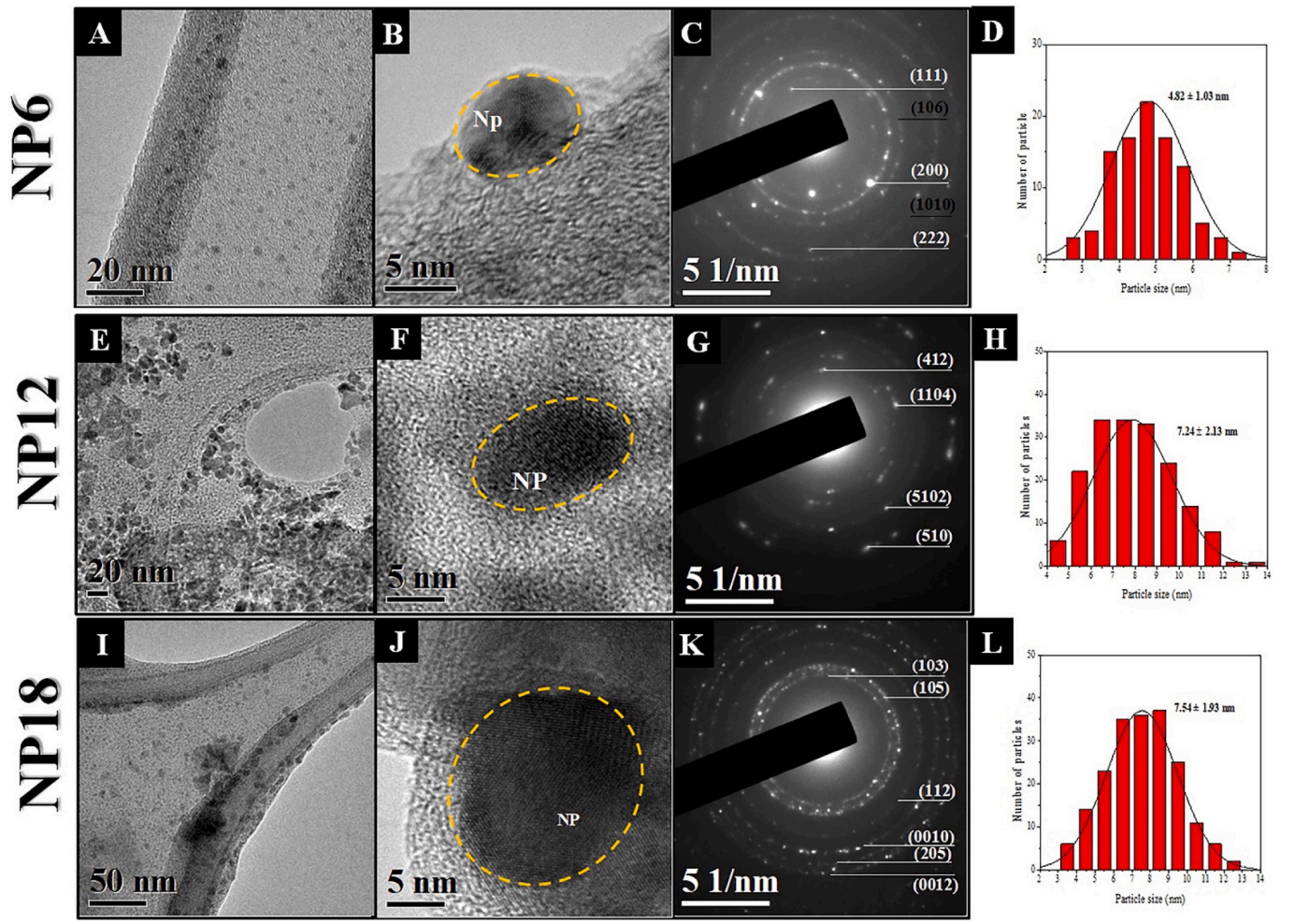

Fig. 5. Micrographs of Cu_xS-NP recent synthesized samples for NP6 (A–D), NP12 (E–H), and NP18 (I–L) samples: TEM capture under low magnification (A, E, and I), HRTEM obtained at high magnification (B, F, and J), SAED patterns (C, G, and K), and size distribution histograms (D, H and L) for each sample.

Table 2
Average size (in Å) from TEM micrographs, and band gap (E_g in eV) from Tauc plot, for as synthesized (NP6, NP12, and NP18), and annealed (NP6T, NP12T, and NP18T) Cu_xS-NP samples.

Sample	Average size (Å)	E_g (eV)	Sample	Range size (Å)	E_g (eV)
NP6	4.82 ± 1.03	2.95	NP6T	6–10	3.07
NP12	7.24 ± 2.13	2.99	NP12T	ca. 15	3.01
NP18	7.54 ± 1.93	3.52	NP18T	20–30	2.86

However, carbon chains major than 12-carbon atoms do not allow the assembly of more copper sulfide moiety, probably due to diffusion phenomena.

The selected area diffraction patterns (SAED) of Cu_xS-NP nanoparticles show the polycrystalline nature of the materials (Fig. 5C, G, and 5K). The SAED pattern of NP6 sample (Fig. 5C) shows reflections associated with the (106) and (1010) planes of the hexagonal structure of covellite (JCPDS 03–0724), in addition to the planes (111), (202), and (222) related to the cubic digenite (JCPDS 04–0861). In the sample NP12 (Fig. 5G), the diffraction rings are still present with (412), (1104), and (5102) related to the orthorhombic structure of chalcocite (JCPDS 02–1272). The SAED pattern in Fig. 5K revealed that the diffraction rings from inner to outer could be indexed as (103), (105), (112), (0010), (205), and (0012) reflections, corresponding to the hexagonal structure of covellite (JCPDS 65–3929). These results confirm the results observed in X-ray diffraction analyses (*vide supra*).

At this point, the main objective of the work has been accomplished. The reaction of the N-alkyldithiocarbamatecopper(II) complex with $NaBH_4$ yields copper sulfide nanoparticles with DTC ligands upon their surface. The presence of DTC helps to control the size and morphology of the particles, as been designed. In all the reported cases, the preparation of the Cu_xS-NP form dithiocarbamatecopper(II) complexes completely degrades the precursor. The nanoparticles obtained need to be capped with surfactants or amines of large carbon chains. In our methodology, decomposition of the N-alkyl dithiocarbamate generates the Cu_xS-NP with a remaining DTC molecule surface bonded. This is the first report of a surface-modified Cu_xS-NP process using a single-source precursor in a one-step synthesis, as far as we know. However, a subproduct (tincalconite) affects the purity of the sample and must be removed.

3.5. *Thermal analyses of Cu_xS-NP*

Accordingly, the reaction of $NaBH_4$ produces tincalconite as an undesired subproduct. The solubility was the first approach to purify the copper sulfide and remove borates. Copper sulfide is water-insoluble and slightly soluble in HCl and NH_4OH. On the other side, tincalconite increases its solubility in dehydrated forms at temperatures higher than 50 °C [46]. Therefore, the washes with water and ethanol failed to purify the Cu_xS-NP from the tincalconite [47].

The second approach was a thermal treatment to eliminate or decompose the tincalconite phase. Borates are thermally stable mineral compounds up to 1000 °C, and when acquiring this temperature, boron

evaporates. Copper sulfide melts at 1130 °C. However, DTC ligands decompose at temperatures around 200 °C. Therefore, the elimination of borates through a heat treatment would result in the total degradation of the compounds forming the particles. The borates are hard to remove at lower temperatures. However, tincalconite loses its crystallinity by dehydration between 25 and 250 °C [48], with the first dehydration around 149 °C [49], producing an amorphous material [50]. In this sense, the thermal treatment of the samples has been proposed to adequately characterize the Cu_xS phases using x-ray diffraction without carrying out a more complicated process of purification of the samples.

Our Cu_xS preparation is not a thermal method, therefore applying high temperatures for the refinement of the reaction mixture would fail its novelty. Due to the missing purification of the Cu_xS phases, we suggest dehydrating tincalconite by a short treatment over 100 °C. Therefore, it would be likely to characterize the copper sulfide phases, avoiding as far as possible the DTC molecule decomposition. To achieve this, thermal analyses of the Cu_xS-NP samples give some insights into the annealing process.

The thermal properties of the Cu_xS-NP were studied by thermogravimetric analyses (TGA) and differential scan calorimetry (DSC) techniques, in a nitrogen atmosphere (Fig. 6 and 7). For the NP6 sample, the TGA analysis shows three important steps (Fig. 6). (a) The first stage is a slight loss (<2%) at a temperature > 100 °C, due to the loss of adsorbed solvent molecules. The DSC profile shows an endothermic peak centered at 80 °C, corresponding to absorbed ethanol molecules, which is the solvent used on the preparation. (b) Above 100 °C, the TGA shows further weight loss (ca. 20%w), assigned to the dehydration of tincalconite (100–200 °C) [51]. The DSC curve shows two endotherm peaks centered at 132 and 154 °C, associated with the loss of structural water molecules of borates [52] (c) A TGA weight loss (ca. 20 %w). between 200 and 300 °C is assigned to the decomposition of the DTC molecules. A broad DSC endotherm at 244 °C could be associated with the decomposition of DTC molecules with different interaction modes on the Cu_xS-NP surface [43,53,54].

It is important to note that the thermal profile is similar between NP6, NP12, and NP18 samples (Fig. 7). In all the cases, the three stages of TGA curves are present, with differences only in the weight % of the loss, but in the same temperature range. There is a relation of the carbon chain large with the relative amount of tincalconite and DTC molecules, that follow the order: NP6 > NP12 > NP18. The shorter DTC carbon chain, the higher number of borates in the Cu_xS-NPs, by the better diffusion of the reactants in short carbon atoms of the DTC molecule. On the other side, larger carbon chains produce fewer DTC molecules over Cu_xS-NPs. With the small size of the Cu_xS-NPs, fewer DTC molecules surround the nanoparticles.

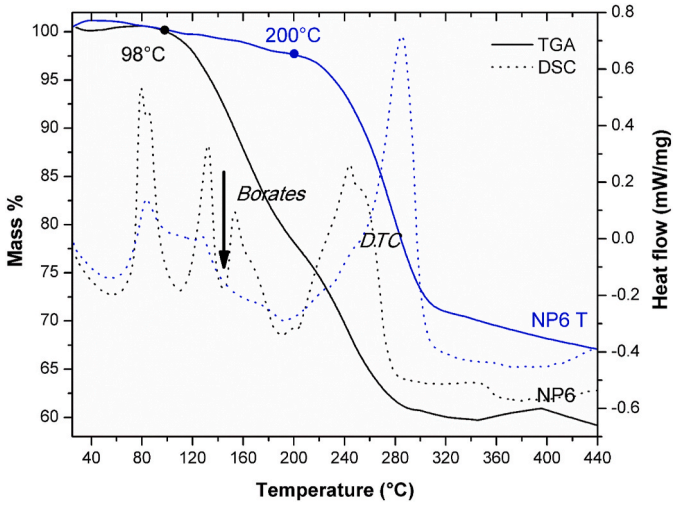

Fig. 6. TGA and DSC analyses of NP6 and NP6T in nitrogen atmosphere.

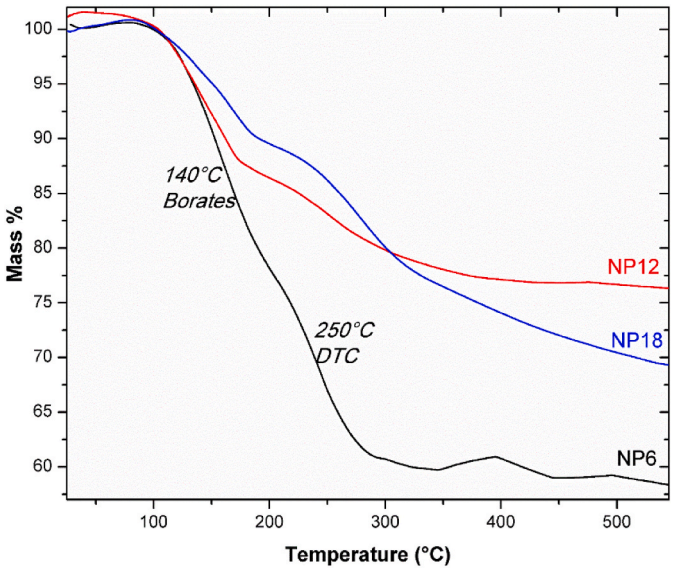

Fig. 7. TGA comparison of NP6, NP12 and NP18 showing the similar profile of the thermograms.

At this point, the tincalconite can be dehydrated with a thermal treatment at a temperature <200 °C, producing an amorphous phase [50]. It could help us to characterize the Cu_xS phases in our material. It is important to apply temperatures minor than 200 °C avoiding DTC decomposition. For this reason, the Cu_xS-NPs samples were annealed at 180 °C during only 10 min dehydrating tincalconite phase. For NP6, the annealing should be limited to 5 min to avoid the formation of copper sulfates from the thermal decomposition of Cu_xS [55].

3.6. *Annealing of the Cu_xS-NP samples*

Consequently, the annealing of the samples at 180 °C allows us to identify the Cu_xS phases without DTC ligands loss, which prevents the particle coalescence. Despite the annealing, DTC ligands remain in the Cu_xS-NP. In the IR spectra of annealing samples (NP6T, NP12T, and NP18T in Fig. 8), the tincalconite signals vanish or reduce their intensity, but the dithiocarbamate remains, as seen by the peaks on 2910, 2850, and 1420 cm^{-1}.

The annealing of Cu_xS-NP samples produces significant changes in the PXRD. The NP6T, NP12T, and NP18T diffractograms (Figs. 2–4) dramatically modify their crystalline shape to develop broad signals more related to the nanoparticle presence. These facts allow us to find the Cu_xS phases of each sample because the tincalconite peaks have vanished. The NP6T, NP12T, and NP12T samples have only two copper sulfides phases: a digenite even in all the cases (Cu_9S_5, JCPDS 04–0861), and a different Cu_xS phase: (a) covellite (CuS, JCPDS 03–0724) for NP6T, with higher intensity than digenite peaks, (b) chalcocite (Cu_2S, JCPDS 02–1272) for NP12T, in low quantity respecting digenite, and (c) covellite (CuS, JCPDS 65–3929) for NP18T, with the same intensity of digenite. Covellite phases on NP6T and NP18T have different structures, probably due to a completely different preferred orientation. The calculated crystallite size for the most intense not overlapped peaks of each sample (Table 3) shows that the particles agree to nanometric dimensions.

After the heat treatment, the particles remain the nanometric size (Fig. 9). The annealing promotes the nanoparticle size increase (Table 3) because of the decomposition of some DTC molecules. The amorphous coating disappears: no halo can be detected on the TEM and HRTEM micrographs as before annealed.

On the other hand, the morphology of the NP6T remains quasi-spherical, forming some clusters without agglomeration (Fig. 8B).

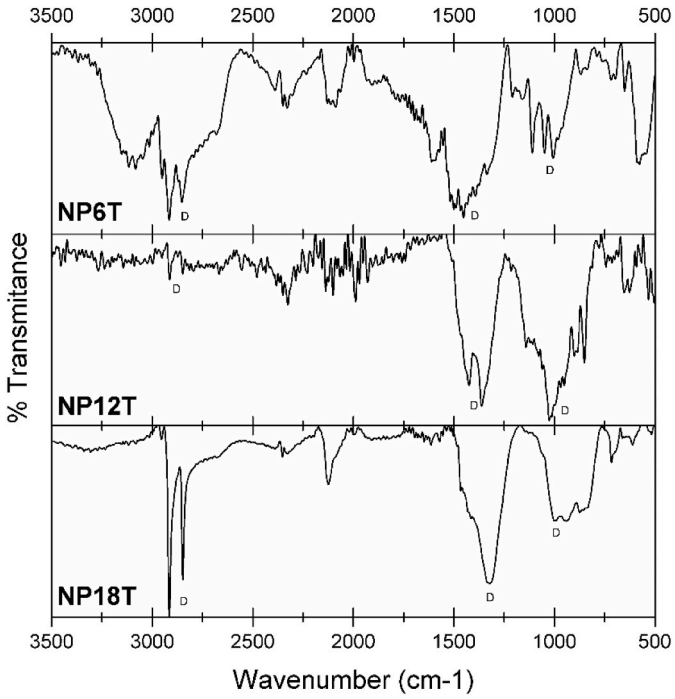

Fig. 8. *IR spectra of Cu_xS-NP annealed NP6T, NP12T, and NP18T samples at 180°C @* 10 min.

Table 3
Average crystallite size calculated by Scherrer formula for representative peaks of Cu_xS-NP sample.

Sample	2Theta (°)	Cu_xS Phase	hkl	Crystallite (nm)
NP6T	29.27	Cov (03–0724)	(2 0 2)	11.8
	46.58	Dig (04–0861)	(2 2 0)	7.4
	47.93	Cov (03–0724)	(1 1 0)	10.54
	52.63	Cov (03–0724)	(1 0 8)	7.49
	59.17	Cov (03–0724)	(1 1 6)	7.29
			Average:	*8.90*
NP12T	37.54	Chall (02–1272)	(1 10 4)	9.7
	48.15	Chall (02–1272)	(1 14 2)	4.6
	54.26	Dig (04–0861)	(3 1 1)	8.6
			Average:	*7.63*
NP18T	21.54	Cov (65–3929)	(0 0 4)	6.18
	46.09	Dig (04–0861)	(2 2 0)	8.96
	54.49	Dig (04–0861)	(3 1 1)	9.99
			Average:	*8.38*

Ellipsoids are the predominant morphology of NP12T (Fig. 9D). The most significant change in morphology is for NP18T: the TEM and HRTEM micrographs (Fig. 9G and H) show a cuboctahedron morphology, one of the most stable for Cu_xS nanostructures [56]. The annealed Cu_xS-NP SAED (Fig. 9C, F, and 9I) displays the polycrystalline nature of the material. NP6T SAED (Fig. 9C) presents different diffraction rings that are related to the (004), (110), and (116) planes of the hexagonal covellite (JCPDS 03–0724) and the (220) plane of the cubic structure of digenite phase (JCPDS 04–0861). For the NP12T sample, the diffraction pattern shows the single-crystalline structure of the nanoparticle, and the spots are related to the (1142) plane of the orthorhombic chalcocite (Fig. 8F). The SAED pattern of NP18T (Fig. 8I) shows the polycrystallinity of the nanoparticles obtained. The diffraction rings correlate with the (008) and (0014) planes of the hexagonal covellite (JCPDS 65–3929). Additionally, diffractions of planes {004} of the covellite were observed. This phase can be related to the cuboctahedron morphology observed in TEM micrography.

The annealing improves the thermal stability of Cu_xS-NPs up to 200 °C from 98 °C, on the recent synthesized samples, as can be noticed in the TGA curve of NP6T (Fig. 6). The TGA curve shows the loss of ethanol and structural water remanent (ca. 3 w%), which could be related to two endotherm peaks in the DSC profile at 82, and 127 °C, respectively (Fig. 6). DTC molecules are not eliminated with the annealing from the Cu_xS-NPs surface. The NP6T TGA curve shows a weight loss of ca. 20% between 200 and 320 °C corresponding to the decomposition of DTC, similar to the NP6 sample. However, the endotherm observed in the DSC profile is shifted toward higher temperatures from the sample without thermal treatment (285 °C for NP6T, and 240 °C for NP6), probably due to the energy increase on the interactions DTC-Cu_xS.

3.7. The band gap of the Cu_xS-NP

As a good semiconductor material, the Cu_xS-NP has the energy band gap (E_g) in the border of visible and Ultraviolet regions (Fig. 10 and Table 2). The energy band gap was calculated by the Tauc plot using the baseline approach [57]. Copper sulfide is considered as a direct band gap semiconductor, as stated by Lukashev [58]. The E_g values are similar to those reported for Cu_xS materials [59,60]. It is important to note that NP12 and NP12T show similar E_g values (2.99 vs. 3.01 eV). In the case of NP6 and NP6T, there is a slight blue shift of band gap values (2.95 and 3.07 eV, respectively), which has been associated with a decrease in the grain size [61]. Additionally, the E_g values for NP18 and NP18T (3.52 vs. 2.86 eV) have a redshift, probably due to the increase of the grain size. The nanoparticles modified with ligands decrease their band gap [62] and require more energy to produce h^+/e^- pair. In this case, the annealing of NP18 causes a partial loss of DTC around the nanoparticles, improving their optical properties by reducing their band gap. In the same sense, the length of the DTC carbon chain in NP18 could cause a long distance between the nanoparticles that need more energy to promote the electron to the conduction band. For all our samples, the estimated band gap energy is blue-shifted respecting the value of 1.2 eV band gap of the bulk copper sulfide [63]. The band gap is probably increased by the quantum size effect against the bulk copper sulfide semiconductor. This behavior could be ascribed to the small crystallite sizes of the nanoparticle [64,65].

4. Conclusions

Chemical decomposition of the N-alkyldithiocarbamatecopper(II) complexes by $NaBH_4$ reaction is an efficient way to obtain copper sulfide nanoparticles from a single-source precursor without thermal conditions. The principal advantage of the strategy is that DTC molecules remain in the Cu_xS-NP as capping agent achieving homogeneous morphology, furthermore the large alkyl chain of the DTC can be used to control the size of the particles. The obtained Cu_xS-NPs have two phases: a digenite (Cu_9S_5) in all cases, and chalcocite (Cu_2S) or covellite (CuS) depending on the chain length used. The band gap of the Cu_xS-NP in the border of visible and UV regions confirms the semiconductor nature of the materials and strong quantum confinement. However, the use of borohydride ions produces an undesirable byproduct (tincalconite) hard to eliminate. In this sense, new research is under study. This new synthetic approach has the potential to obtain metal sulfide nanoparticles with DTC molecules around particle surface, which increase the potential applications of the Cu_xS nanoparticles in composites, monolayers, or nanofluids.

CRediT authorship contribution statement

Eder I. Duran-García: Conceptualization, All authors contributed to the study conception and design, Data curation, Formal analysis, Material preparation, data collection and analysis were performed, all authors commented on previous versions of the manuscript, All authors read and approved the final manuscript. **José Martínez-Santana:** Conceptualization, All authors contributed to the study conception and

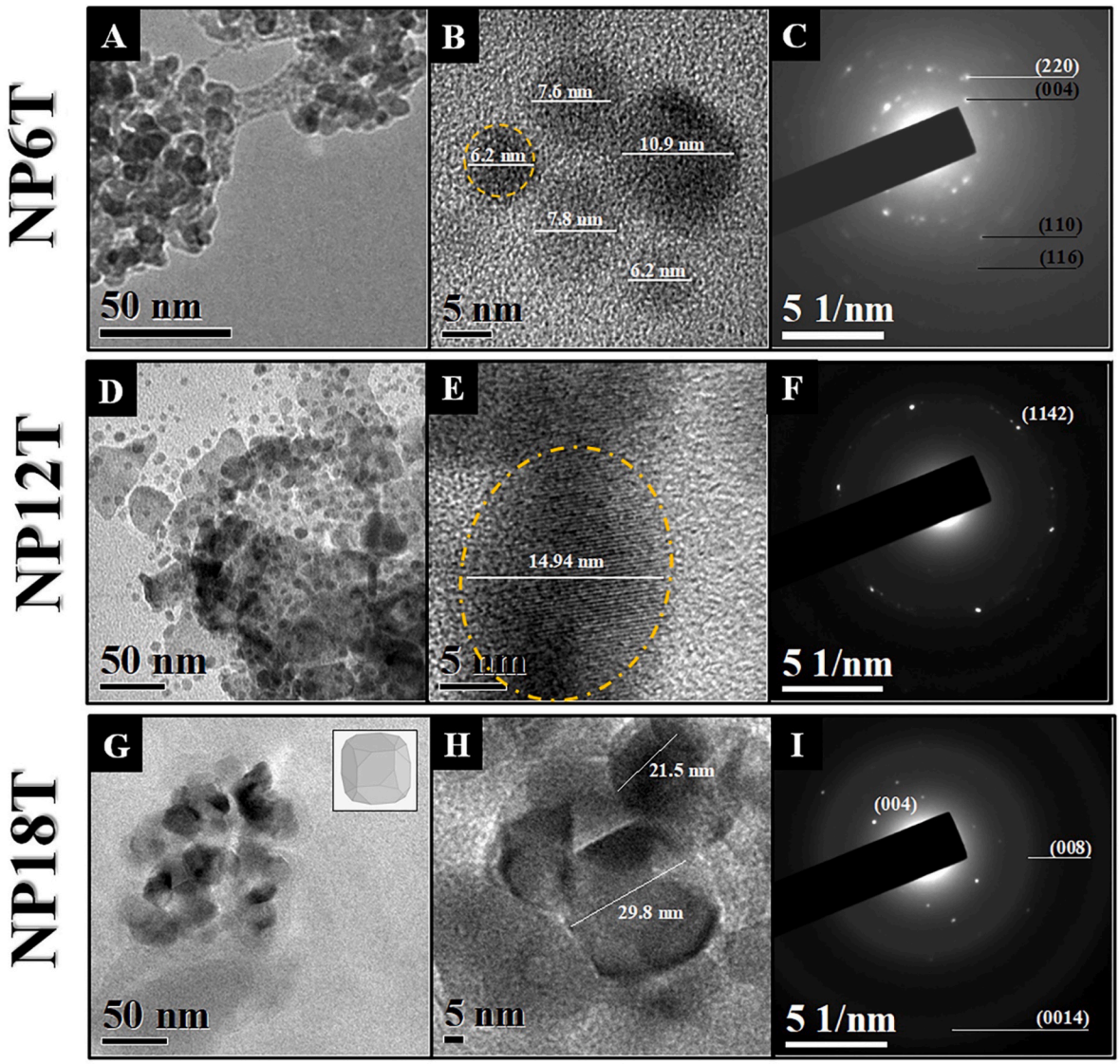

Fig. 9. Cu_xS-NP after annealing: TEM Micrograph (A, D, and G), HRTEM micrograph (B, E, and H), and SAED pattern (C, F, and I). NP18T shows cuboctahedron morphology (example insert in G).

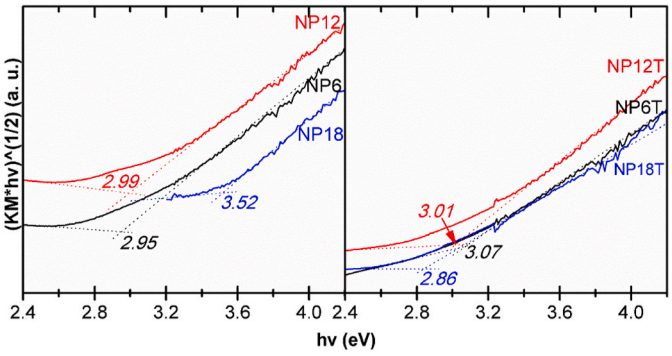

Fig. 10. Tauc plot of NP and NPT samples, showing the band gap (E_g) value calculated by Tauc baseline method.

design, Data curation, Formal analysis, Material preparation, data collection and analysis were performed, Writing – original draft, The first draft of the manuscript was written, all authors commented on previous versions of the manuscript, All authors read and approved the final manuscript. **Nayely Torres-Gómez:** Conceptualization, All authors contributed to the study conception and design, Data curation, Formal analysis, Material preparation, data collection and analysis were performed, all authors commented on previous versions of the manuscript, All authors read and approved the final manuscript. **Alfredo R. Vilchis-Nestor:** Conceptualization, All authors contributed to the study conception and design, all authors commented on previous versions of the manuscript, All authors read and approved the final manuscript. **Iván García-Orozco:** Conceptualization, All authors contributed to the study conception and design, Writing – original draft, The first draft of the manuscript was written, all authors commented on previous versions of the manuscript, Funding acquisition, was done, All authors read and approved the final manuscript.

Declaration of competing interest

The authors declare that they have no known competing financial interests or personal relationships that could have appeared to influence the work reported in this paper.

Acknowledgments

This research was supported by Universidad Autónoma del Estado de

México project SIEA-UAEMex 4358/2017/CI and the scholarship (J. M.-S. and E. D.-G.) by Consejo Nacional de Ciencia y Tecnología CONACYT No. 520172 and 936186. Authors thank the invaluable technical assistance of Uvaldo Hernández, Citlalit Martínez, Alejandra Nuñez, Lizbeth Triana, and Jesús Velázquez in the characterization techniques.

References

[1] X. Wang, Z. Fang, X. Lin, Copper sulfide nanotubes: facile, large-scale synthesis, and application in photodegradation, J. Nanoparticle Res. 11 (3) (2009) 731–736, https://doi.org/10.1007/s11051-008-9480-2.

[2] W. Gao, Y. Sun, M. Cai, Y. Zhao, W. Cao, Z. Liu, G. Cui, B. Tang, Copper sulfide nanoparticles as a photothermal switch for TRPV1 signaling to attenuate atherosclerosis, Nat. Commun. 9 (1) (2018) 231, https://doi.org/10.1038/s41467-017-02657-z.

[3] K.B.A. Ahmed, V. Anbazhagan, Synthesis of copper sulfide nanoparticles and evaluation of in vitro antibacterial activity and in vivo therapeutic effect in bacteria-infected zebrafish, RSC Adv. 7 (58) (2017) 36644–36652, https://doi.org/10.1039/C7RA05636B.

[4] J. Hou, X. Zhou, Z. Yang, H. Nie, The electrochemical synthesis of CNTs/N-Cu2S composites as efficient electrocatalysts for water oxidation, J. Nanoparticle Res. 22 (1) (2020) 12, https://doi.org/10.1007/s11051-019-4729-5.

[5] S. Goel, F. Chen, W. Cai, Synthesis and biomedical applications of copper sulfide nanoparticles: from sensors to theranostics, Small 10 (4) (2014) 631–645, https://doi.org/10.1002/smll.201301174.

[6] U. Shamraiz, R.A. Hussain, A. Badshah, Fabrication and applications of copper sulfide (CuS) nanostructures, J. Solid State Chem. 238 (2016) 25–40, https://doi.org/10.1016/j.jssc.2016.02.046.

[7] R.S. Mane, C.D. Lokhande, Chemical deposition method for metal chalcogenide thin films, Mater. Chem. Phys. 65 (1) (2000) 1–31, https://doi.org/10.1016/S0254-0584(00)00217-0.

[8] K. Tezuka, W.C. Sheets, R. Kurihara, Y.J. Shan, H. Imoto, T.J. Marks, K. R. Poeppelmeier, Synthesis of covellite (CuS) from the elements, Solid State Sci. 9 (1) (2007) 95–99, https://doi.org/10.1016/j.solidstatesciences.2006.10.002.

[9] I. Ancutienė, V. Janickis, Formation and characterization of CuxS layers on polyethylene film using the solutions of sulfur in carbon disulfide, Open Chem 8 (6) (2010) 1281–1287, https://doi.org/10.2478/s11532-010-0104-1.

[10] M. Ramya, S. Ganesan, Influence of thickness and temperature on the properties of Cu2S thin films, Iran. J. Sci. Technol. Sci. 37 (3) (2013) 293–300, https://doi.org/10.22099/ijsts.2013.1606.

[11] Y. Lou, X. Chen, A.C. Samia, C. Burda, Femtosecond spectroscopic investigation of the carrier lifetimes in digenite quantum dots and discrimination of the electron and hole dynamics via ultrafast interfacial electron transfer, J. Phys. Chem. B 107 (45) (2003) 12431–12437, https://doi.org/10.1021/jp035618k.

[12] N.L. Botha, P.A. Ajibade, Effect of temperature on crystallite sizes of copper sulfide nanocrystals prepared from copper(II) dithiocarbamate single source precursor, Mater. Sci. Semicond. Process. 43 (2016) 149–154, https://doi.org/10.1016/j.mssp.2015.12.006.

[13] M.D. Khan, M. Akhtar, M.A. Malik, N. Revaprasadu, P. O'Brien, New examples of phase control in the preparation of copper sulfide nanoparticles and deposition of thin films by AACVD from bis(Piperidinedithiocarbamato)Copper(II) complex, ChemistrySelect 3 (11) (2018) 2943–2950, https://doi.org/10.1002/slct.201703069.

[14] A.T. Odularu, P.A. Ajibade, Dithiocarbamates: challenges, control, and approaches to excellent yield, characterization, and their biological applications, Bioinorgan. Chem. Appl. 2019 (2019), e8260496, https://doi.org/10.1155/2019/8260496.

[15] P.B. Mann, I.J. McGregor, S. Bourke, M. Burkitt-Gray, S. Fairclough, M.T. Ma, G. Hogarth, M. Thanou, N. Long, M. Green, An atom efficient, single-source precursor route to plasmonic CuS nanocrystals, Nanoscale Adv 1 (2) (2019) 522–526, https://doi.org/10.1039/C8NA00325D.

[16] P.A. Ajibade, B.M. Sikakane, N.L. Botha, A.E. Oluwalana, B. Omondi, Synthesis and crystal structures of bis(dibenzyl dithiocarbamato)Cu(II) and Ag(I) complexes: precursors for Cu1.8S and Ag2S nano-photocatalysts, J. Mol. Struct. 1221 (2020) 128791, https://doi.org/10.1016/j.molstruc.2020.128791.

[17] N. ul Ain, Zia-ur-Rehman, A. Aamir, Y. Khan, M. Rehman, D.-J. Lin, Catalytic and photocatalytic efficacy of hexagonal CuS nanoplates derived from copper(II) dithiocarbamate, Mater. Chem. Phys. 242 (2020) 122408, https://doi.org/10.1016/j.matchemphys.2019.122408.

[18] N.L. Botha, P.A. Ajibade, Optical and structural characterization of copper sulphide nanoparticles from copper(II) piperidine dithiocarbamate, Opt. Quant. Electron. 52 (7) (2020) 337, https://doi.org/10.1007/s11082-020-02455-w.

[19] L.H. van Poppel, T.L. Groy, M.T. Caudle, Carbon−Sulfur bond cleavage in Bis(N-Alkyldithiocarbamato)Cadmium(II) Complexes: heterolytic desulfurization coupled to topochemical proton transfer, Inorg. Chem. 43 (10) (2004) 3180–3188, https://doi.org/10.1021/ic035135v.

[20] A.A. Memon, M. Afzaal, M.A. Malik, C.Q. Nguyen, P. O'Brien, J. Raftery, The N-alkyldithiocarbamato complexes [M(S2CNHR)2] (M = Cd(II) Zn(II); R = C2H5, C4H9, C6H13, C12H25); their synthesis, thermal decomposition and use to prepare of nanoparticles and nanorods of CdS, Dalton Trans. 37 (2006) 4499–4505, https://doi.org/10.1039/B606661E.

[21] C.E. Morrison, F. Wang, N.P. Rath, B.M. Wieliczka, R.A. Loomis, W.E. Buhro, Cadmium bis(phenyldithiocarbamate) as a nanocrystal shell-growth precursor, Inorg. Chem. 56 (21) (2017) 12920–12929, https://doi.org/10.1021/acs.inorgchem.7b01711.

[22] N. Hollingsworth, A. Roffey, H.-U. Islam, M. Mercy, A. Roldan, W. Bras, M. Wolthers, C.R.A. Catlow, G. Sankar, G. Hogarth, N.H. de Leeuw, Active nature of primary amines during thermal decomposition of nickel dithiocarbamates to nickel sulfide nanoparticles, Chem. Mater. 26 (21) (2014) 6281–6292, https://doi.org/10.1021/cm503174z.

[23] F.F. Bobinihi, J. Osuntokun, D.C. Onwudiwe, Syntheses and characterization of nickel(II) dithiocarbamate complexes containing NiS4 and NiS2PN moieties: nickel sulphide nanoparticles from a single source precursor, J. Saudi Chem. Soc. 22 (4) (2018) 381–395, https://doi.org/10.1016/j.jscs.2017.10.001.

[24] A.M. Paca, P.A. Ajibade, Synthesis, optical, and structural studies of iron sulphide nanoparticles and iron sulphide hydroxyethyl cellulose nanocomposites from bis-(Dithiocarbamato)Iron(II) single-source precursors, Nanomaterials 8 (4) (2018) 187, https://doi.org/10.3390/nano8040187.

[25] D.C. Onwudiwe, T. Arfin, C.A. Strydom, R.J. Kriek, A study of the thermal and AC impedance properties of N-phenyldithiocarbamate complexes of Zn(II), Electrochim. Acta 109 (2013) 809–817, https://doi.org/10.1016/j.electacta.2013.07.176.

[26] D.C. Onwudiwe, C.A. Strydom, The bipyridine adducts of N-phenyldithiocarbamato complexes of Zn(II) and Cd(II); synthesis, spectral, thermal decomposition studies and use as precursors for ZnS and CdS nanoparticles, Spectrochim. Acta. A. Mol. Biomol. Spectrosc. 135 (2015) 1080–1089, https://doi.org/10.1016/j.saa.2014.08.004.

[27] J. Seo, S. Lee, B. Koo, W. Jung, Controlling the size of Pt nanoparticles with a cationic surfactant, CnTABr. *CrystEngComm* 20 (14) (2018) 2010–2015, https://doi.org/10.1039/C7CE02235B.

[28] L.P. Singh, S.K. Bhattacharyya, G. Mishra, S. Ahalawat, Functional role of cationic surfactant to control the nano size of silica powder, Appl. Nanosci. 1 (3) (2011) 117–122, https://doi.org/10.1007/s13204-011-0016-1.

[29] U. Klekotka, D. Satuła, A. Basa, B. Kalska-Szostko, Importance of surfactant quantity and quality on growth regime of iron oxide nanoparticles, Materials 13 (7) (2020) 1747, https://doi.org/10.3390/ma13071747.

[30] J.P. Wilcoxon, P.P. Provencio, Use of surfactant micelles to control the structural phase of nanosize iron clusters, J. Phys. Chem. B 103 (45) (1999) 9809–9812, https://doi.org/10.1021/jp992133g.

[31] W. Lou, M. Chen, X. Wang, W. Liu, Size control of monodisperse copper sulfide faceted nanocrystals and triangular nanoplates, J. Phys. Chem. C 111 (27) (2007) 9658–9663, https://doi.org/10.1021/jp070166n.

[32] N. Torres-Gomez, A.R. Vilchis-Nestor, R.M. Gomez-Espinosa, I. Garcia-Orozco, Synthesis and characterization of copper(II) complexes with long chain dithiocarbamates, Adv. Mater. Res. 976 (2014) 164–168. https://doi.org/10.4028/www.scientific.net/AMR.976.164.

[33] G. Sailaja, S. Nowshuddin, M.N.A. Rao, Sodium borohydride efficiently removes copper from amino acid–copper complexes, Tetrahedron Lett. 45 (50) (2004) 9297–9298, https://doi.org/10.1016/j.tetlet.2004.10.060.

[34] V.R. Fernandes, A.M.F.R. Pinto, C.M. Rangel, Hydrogen production from sodium borohydride in methanol–water mixtures, Int. J. Hydrogen Energy 35 (18) (2010) 9862–9868, https://doi.org/10.1016/j.ijhydene.2009.11.064.

[35] G.M. Arzac, A. Fernández, Hydrogen production through sodium borohydride ethanolysis, Int. J. Hydrogen Energy 40 (15) (2015) 5326–5332, https://doi.org/10.1016/j.ijhydene.2015.01.115.

[36] K. Eschliman, S.H. Bossmann, Synthesis of isothiocyanates: an update, Synthesis 51 (8) (2019) 1746–1752, https://doi.org/10.1055/s-0037-1612303.

[37] A.W. Wills, M.S. Kang, A. Khare, W.L. Gladfelter, D.J. Norris, Thermally degradable ligands for nanocrystals, ACS Nano 4 (8) (2010) 4523–4530, https://doi.org/10.1021/nn100637u.

[38] N.-Q. Zhou, L.-J. Tian, Y.-C. Wang, D.-B. Li, P.-P. Li, X. Zhang, H.-Q. Yu, Extracellular biosynthesis of copper sulfide nanoparticles by shewanella oneidensis MR-1 as a photothermal agent, Enzym. Microb. Technol. 95 (2016) 230–235, https://doi.org/10.1016/j.enzmictec.2016.04.002.

[39] A. Tang, S. Qu, K. Li, Y. Hou, F. Teng, J. Cao, Y. Wang, Z. Wang, One-pot synthesis and self-assembly of colloidal copper(I) sulfide nanocrystals, Nanotechnology 21 (28) (2010) 285602, https://doi.org/10.1088/0957-4484/21/28/285602.

[40] S. De, S. Mandal, Surfactant-assisted shape control of copper nanostructures, Colloids Surf. Physicochem. Eng. Asp. 421 (2013) 72–83, https://doi.org/10.1016/j.colsurfa.2012.12.035.

[41] Infrared Spectroscopy, Fundamentals and applications, Wiley, https://www.wiley.com/en-mx/Infrared+Spectroscopy%3A+Fundamentals+and+Applications-p-9780470854280. (Accessed 6 August 2020).

[42] S. Khan, S.A.A. Nami, K.S. Siddiqi, Piperazine pivoted transition metal dithiocarbamates, J. Mol. Struct. 875 (1) (2008) 478–485, https://doi.org/10.1016/j.molstruc.2007.05.020.

[43] K.S. Siddiqi, S.A.A. Nami, Lutfullah, Y. Chebude, Template synthesis of symmetrical transition metal dithiocarbamates, J. Braz. Chem. Soc. 17 (1) (2006) 107–112, https://doi.org/10.1590/S0103-50532006000100016.

[44] G. Yang, S. Chai, X. Xiong, S. Zhang, L. Yu, P. Zhang, Preparation and tribological properties of surface modified Cu nanoparticles, Trans. Nonferrous Metals Soc. China 22 (2) (2012) 366–372, https://doi.org/10.1016/S1003-6326(11)61185-0.

[45] W.P. Lim, C.T. Wong, S.L. Ang, H.Y. Low, W.S. Chin, Phase-selective synthesis of copper sulfide nanocrystals, Chem. Mater. 18 (26) (2006) 6170–6177, https://doi.org/10.1021/cm061686i.

[46] J. Andrieux, L. Laversenne, O. Krol, R. Chiriac, Z. Bouajila, R. Tenu, J.J. Counioux, C. Goutaudier, Revision of the NaBO2–H2O phase diagram for optimized yield in the H2 generation through NaBH4 hydrolysis, Int. J. Hydrogen Energy 37 (7) (2012) 5798–5810, https://doi.org/10.1016/j.ijhydene.2011.12.106.

[47] E. Moroydor Derun, N. Tugrul, F.T. Senberber, A.S. Kipcak, S. Piskin, The Optimization of Copper Sulfate and Tincalconite Molar Ratios on the Hydrothermal Synthesis of Copper Borates, 2014, https://doi.org/10.5281/zenodo.1096563.
[48] M.F. Gazulla, M.P. Gómez, M. Orduña, G. Silva, Caracterización química, mineralógica y térmica de boratos naturales y sintéticos, Bol. Soc. Esp. Cerámica Vidr. 44 (1) (2005) 21–31, https://doi.org/10.3989/cyv.2005.v44.i1.399.
[49] Sevim, F.; Küçükarslan, H.; Demir, F.; Eroglu, H.; Aktan, M. Dehydration Kinetics of Tincalconite from Thermogravimetric Data. vol. 5.
[50] S. Çoban, B. Özkarasu, F.T. Şenberber, A.S. Kipçak, İ. Doymaz, E.M. Derun, Microwave dehydration modelling OF tincalconite, J. Therm. Eng. 4 (2) (2017) 1803–1812, https://doi.org/10.18186/journal-of-thermal-engineering.382399.
[51] Sevim, F.; Küçükarslan, H.; Demir, F.; Eroglu, H.; Aktan, M. Dehydration Kinetics of Tincalconite from Thermogravimetric Data. vol. 5.
[52] A. Kanturk, M. Sari, S. Synthesis Piskin, Crystal structure and dehydration kinetics of NaB(OH)4·2H2O, Kor. J. Chem. Eng. 25 (6) (2008) 1331–1337, https://doi.org/10.1007/s11814-008-0218-8.
[53] C.G. Sceney, J.F. Smith, J.O. Hill, R.J. Magee, A TG/GC/MS study of copper dimethyl- and diethyldithiocarbamates, J. Therm. Anal. 9 (3) (1976) 415–423, https://doi.org/10.1007/BF01909407.
[54] I.J.-L. Plante, T.W. Zeid, P. Yang, T. Mokari, Synthesis of metal sulfide nanomaterials via thermal decomposition of single-source precursors, J. Mater. Chem. 20 (32) (2010) 6612–6617, https://doi.org/10.1039/C0JM00439A.
[55] G.S. Tyndall, A.R. Ravishankara, Atmospheric oxidation of reduced sulfur species, Int. J. Chem. Kinet. 23 (6) (1991) 483–527, https://doi.org/10.1002/kin.550230604.
[56] S. Gross, A. Vittadini, N. Dengo, Functionalisation of colloidal transition metal sulphides nanocrystals: a fascinating and challenging playground for the chemist, Crystals 7 (4) (2017) 110, https://doi.org/10.3390/cryst7040110.
[57] P. Makuła, M. Pacia, W. Macyk, How to correctly determine the band gap energy of modified semiconductor photocatalysts based on UV–vis spectra, J. Phys. Chem. Lett. 9 (23) (2018) 6814–6817, https://doi.org/10.1021/acs.jpclett.8b02892.
[58] P. Lukashev, W.R.L. Lambrecht, T. Kotani, M. van Schilfgaarde, Electronic and crystal structure of ${\mathrm{Cu}}_{2\ensuremath{-}x}\mathrm{S}$: full-potential electronic structure calculations, Phys. Rev. B 76 (19) (2007) 195202, https://doi.org/10.1103/PhysRevB.76.195202.
[59] A. Ghosh, A. Mondal, A simple electrochemical route to deposit Cu7S4 thin films and their photocatalytic properties, Appl. Surf. Sci. 328 (2015) 63–70, https://doi.org/10.1016/j.apsusc.2014.12.032.
[60] C. Zhang, C. Yan, Z. Xue, W. Yu, Y. Xie, T. Wang, Shape-controlled synthesis of high-quality Cu7S4 nanocrystals for efficient light-induced water evaporation, Small 12 (38) (2016) 5320–5328, https://doi.org/10.1002/smll.201601723.
[61] A.T. Salih, A.A. Najim, A.D. Faisal, Influence of annealing temperature on the structural, morphological, optical and electrical properties of Cu7S4 thin films prepared by chemical bath deposition, J. Inorg. Organomet. Polym. Mater. 30 (6) (2020) 2258–2265, https://doi.org/10.1007/s10904-019-01358-y.
[62] K.A.A. Mary, N.V. Unnikrishnan, R. Philip, Role of surface states and defects in the ultrafast nonlinear optical properties of CuS quantum dots, Apl. Mater. 2 (7) (2014), 076104, https://doi.org/10.1063/1.4886276.
[63] Y. Wu, C. Wadia, W. Ma, B. Sadtler, A.P. Alivisatos, Synthesis and photovoltaic application of copper(I) sulfide nanocrystals, Nano Lett. 8 (8) (2008) 2551–2555, https://doi.org/10.1021/nl801817d.
[64] M. Singh, M. Goyal, K. Devlal, Size and shape effects on the band gap of semiconductor compound nanomaterials, J. Taibah Univ. Sci. 12 (4) (2018) 470–475, https://doi.org/10.1080/16583655.2018.1473946.
[65] D.L. Ferreira, J.C.L. Sousa, R.N. Maronesi, J. Bettini, M.A. Schiavon, A.V.N. C. Teixeira, A.G. Silva, Size-dependent bandgap and particle size distribution of colloidal semiconductor nanocrystals, J. Chem. Phys. 147 (15) (2017) 154102, https://doi.org/10.1063/1.4999093.